Kinetics and Mechanism of the Stereochemical Isomerization of an Arene−Ruthenium Complex of the Atropisomeric Ligand 1,1′-Biphenyl-2,2′-diamine

Susan S. Alguindigue, Masood A. Khan, and Michael T. Ashby*

Department of Chemistry and Biochemistry, The University of Oklahoma, 620 Parrington Oval, Room 208, Norman, Oklahoma 73019

Received May 4, 1999

(η^6-Benzene)(δ/λ-1,1′-biphenyl-2,2′-diamine)chlorometal(II) hexafluorophosphate (**1**; metal = ruthenium, osmium) have been synthesized. The rigid nature of the seven-membered chelate ring formed by the 1,1′-biphenyl-2,2′-diamine (dabp) ligand renders the complexes chiral. The resulting C_1 molecular symmetry of **1**(M=Ru) that we have observed in the solid state by single-crystal X-ray crystallography is preserved in solution on the NMR time scale. The four N−H protons of **1**(M=Ru,Os) are chemically inequivalent in the ^{1}H NMR spectrum at 20 °C. Spin-perturbation NMR experiments in acetone solutions reveal pairwise exchange of the resonances that correspond to the N−H protons on the spin-relaxation time scale. The three mechanisms that would account for such an exchange (atropisomerization of the dabp ligand, inversion of stereochemistry at the metal center, and simultaneous inversion of the stereochemistry at the metal and the ligand) are distinguishable, provided a proper assignment of the four N−H protons can be made in the NMR spectra. Having made that assignment, we conclude from 2D EXSY NMR spectroscopy that the mechanism of exchange is inversion of stereochemistry at the dabp ligand center. This observation contrasts with previous reports that conformational isomers of dabp can be resolved.

Introduction

Optically active transition-metal complexes have proven useful in stoichiometric and catalytic stereoselective syntheses. The present study involves the chiral half-sandwich arene−ruthenium complexes (η^6-benzene)-(δ/λ-1,1′-biphenyl-2,2′-diamine)chlorometal(II) hexafluorophosphate (**1**; metal = Ru, Os), examples of a class of compounds that have played an important historical role in defining the field of optically active transition-metal complexes.[1,2] Brunner and co-workers resolved the first ruthenium compound that was chiral at the metal center,[3] and in the two decades that followed they carried out a comprehensive study of the stereochemistry of ruthenium complexes.[4] Such complexes have also emerged as important players in the field of asymmetric catalysis.[5,6] The mechanisms by which stereoisomers of arene−metal complexes are interconverted are therefore significant.

Low-spin d^6 ruthenium(II) piano-stool complexes are generally stereochemically inert.[2] Furthermore, several metal complexes of the potentially atropisomeric ligand 1,1′-biphenyl-2,2′-diamine (dabp)[7−18] and related ligands[19−21] have been reported, and efforts to resolve conformational isomers have been reportedly successful.[8,9] Therefore, we were surprised to learn during spin-labeling NMR experiments that the lifetime for magnetic inequivalence of the stereochemical halves of the dabp of **1** is about 250 ms at room temperature (e.g., spin transfer is observed on the spin-relaxation time scale). We provide evidence herein that **1** undergoes facial inversion at the dabp ligand center by a mechanism that involves atropisomerization. Alternative mechanisms that involve isomerization of the metal center are ruled out experimentally. The relative kinetics of atropisomerization of **1**(M=Ru) and **1**(M=Os) are discussed in the context of ligand misdirection.[22−24]

(1) Brunner, H. *Adv. Organomet. Chem.* **1980**, *18*, 151.
(2) Consiglio, G.; Morandini, F. *Chem. Rev.* **1987**, *87*, 761.
(3) Brunner, H.; Gastinger, R. G. *J. Chem. Soc., Chem. Commun.* **1977**, 488.
(4) Brunner, H.; Oeschey, R.; Nuber, B. *Organometallics* **1996**, *15*, 3616.
(5) Ohta, T.; Takaya, H.; Kitamura, M.; Nagai, K.; Noyori, R. *J. Org. Chem.* **1987**, *52*, 3174.
(6) Mashima, K.; Kusano, K.; Sato, N.; Matsumura, Y.; Nozaki, K.; Kumobayashi, H.; Sayo, Y.; Hori, Y.; Ishizaki, T.; Akutagawa, S.; Takaya, H. *J. Org. Chem.* **1994**, *59*, 3064.
(7) Radlowski, C.; Liu, C. F.; Kim, C. H.; Choi, S. R.; Jun, M. J. *Polyhedron* **1985**, *4*, 769.
(8) McCullough, F.; Bailar, J. C. *J. Am. Chem. Soc.* **1956**, *78*, 714.
(9) Habu, T.; Bailer, J. C. *J. Am. Chem. Soc.* **1966**, *88*, 1128.
(10) Onaka, S.; Iwamoto, T.; Sasaki, Y.; Fujiwara, S. *Bull. Chem. Soc. Jpn.* **1967**, *40*, 1398.
(11) Kalazai, B. A.; Melson, G. A. *Inorg. Chim. Acta* **1968**, *2*, 186.
(12) Kalazai, B. A.; Melson, G. A. *Inorg. Chim. Acta* **1970**, *4*, 360.
(13) Tanimura, T.; Ito, H.; Fujita, J.; Saito, K.; Hirai, S.; Yamasaki, K. *J. Coord. Chem.* **1973**, *3*, 161.
(14) Jordan, W. T.; Lin, C. Y.; Douglas, B. E. *J. Coord. Chem.* **1973**, *3*, 1.
(15) Micu-Semeniuc, R.; Macaroviici, C.; Bossanyi, M. *Rev. Roum. Chim.* **1974**, *19*, 1157.
(16) Onaka, S. *Nippon Kagaku Kaishi* **1974**, 480.
(17) Jun, M. J.; Choi, S. R. *Bull. Korean Chem. Soc.* **1984**, *5*, 237.
(18) Radlowski, C. A.; Liu, C. F.; Jun, M. J. *Inorg. Chim. Acta* **1984**, *86*, 101.
(19) Jun, M. J.; Choi, S. R. *Bull. Korean Chem. Soc.* **1985**, *6*, 119.
(20) Jun, M. J. *Bull. Korean Chem. Soc.* **1985**, *6*, 238.
(21) Lew, D.; Amer, I. *Tetrahedron: Asymmetry* **1993**, *4*, 2147.
(22) Ashby, M. T.; Govindan, G. N.; Grafton, A. K. *J. Am. Chem. Soc.* **1994**, *116*, 4801.
(23) Ashby, M. T. *J. Am. Chem. Soc.* **1995**, *117*, 2000.

10.1021/om990332g CCC: $18.00
Publication on Web 11/05/1999

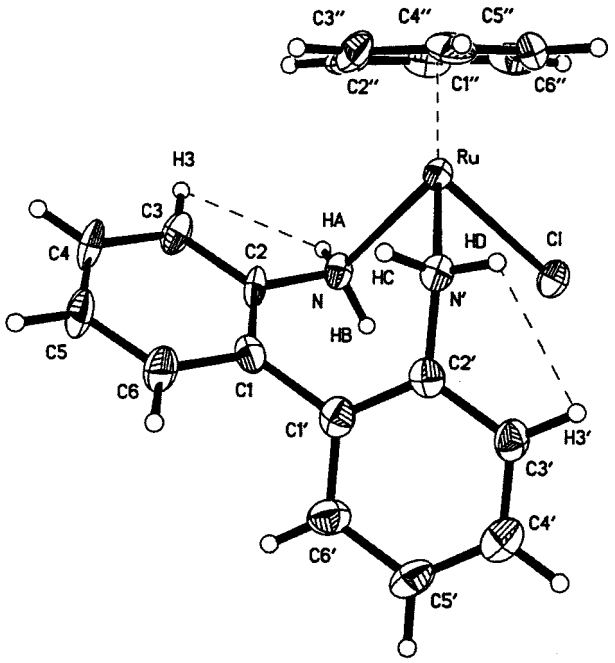

Figure 1. Molecular structure of **1**(M=Ru) showing the atom-labeling scheme and the thermal vibration ellipsoids (50% probability). The labeling scheme of the hydrogen atoms on N and N′ is the same one used in the discussion of the NMR experiment. The dashed lines are the close contacts that are referred to in the discussion of the NOESY experiments.

Results

Solution and Solid-State Structures of 1(M=Ru). The rigid nature of the seven-membered chelate ring formed by the diamine ligand renders **1** chiral. This is clearly seen in the molecular structure that was determined by single-crystal X-ray crystallography (Figure 1). In fact, **1**(M=Ru) spontaneously resolves and crystallizes in a chiral space group ($P2_12_12_1$). In acetone solution, the four hydrogen atoms that are bound to the two nitrogen atoms of **1** are chemically inequivalent in the ^{1}H NMR spectrum at 20 °C. Thus, the C_1 molecular symmetry of **1** that we have observed in the solid state is preserved in solution.

Assignment of the NMR Spectra of 1(M=Ru,Os). Guided by the solid-state structure of **1**(M=Ru) (Figure 1) and the 2D NMR spectra (Figure 2) we have assigned the ^{1}H NMR spectra of **1**. The COSY spectra clearly reveal the *J*-coupling scheme of **1** and thus the connectivity. However, interpretation of the spin-labeling NMR experiments requires an absolute assignment of the ^{1}H resonances, and in particular the spatial relationship between the hydrogen atoms bound to the nitrogens must be determined (vide infra). A study of the ^{1}H NMR spectrum of **1**(M=Ru) reveals three N−H resonances at lower frequency (7.6−8.8 ppm) relative to one that is at higher frequency (4.6 ppm). We assign the unique resonance to H_B (Figure 1). The other three hydrogens (H_A, H_C, and H_D) are in similar environments with respect to shielding by the η^6-arene and biphenyl moieties.[25] The spatial relationship of H_{A-D} is indicated by the 2D NOESY spectrum, which suggests close contacts between H_A-H_3 and $H_D-H_{3'}$ (Figures 1 and 3). The other NOE contacts in the spectrum are consistent with the assignments made from the COSY spectrum. Importantly, the chemical shifts of H_{A-D} are very temperature dependent (Figure 4), and the relative chemical shifts of H_C and H_D change upon raising the temperature from −88 °C (the temperature at which the COSY and NOESY spectra were measured) to 20 °C (the temperature at which the EXSY, vide infra, were measured). Fortunately, the temperature dependence is linear (Figure 5), which allows us to make an unambiguous assignment of the ^{1}H NMR spectra of **1**(M=Ru) at 20 °C. The ^{1}H NMR behavior of **1**(M=Os), including the temperature-dependence, is analogous to that observed for **1**(M=Ru).

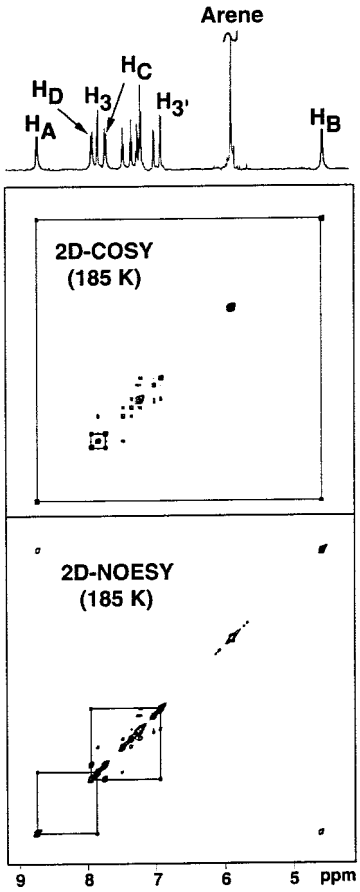

Figure 2. 2D-COSY spectrum of **1**(M=Ru) at 185 K and 500 MHz (top) illustrating the scalar coupling between geminal hydrogens that are bound to N and N′. 2D-NOESY spectrum of **1**(M=Ru) at 185 K (bottom) that illustrates the $H_A\cdots H_3$ and $H_D\cdots H_{3'}$ contacts.

Dynamic Behavior of 1(M=Ru,Os) in Solution. Interestingly, spin-perturbation NMR methods reveal pairwise exchange of the N−H protons of **1** in acetone solution. The three mechanisms that would account for such an exchange (atropisomerization of the 1,1′-biphenyl-2,2′-diamine ligand, inversion of stereochemistry at the metal center, and simultaneous inversion of the stereochemistry at the metal and the ligand) are distinguishable, provided that an assignment of the N−H resonances can be made. Consider first a mechanism that involves inversion of the metal center (Scheme 1). When **1** is viewed conceptually as a tetrahedral molecule with one bidentate ligand, inversion at the metal center involves exchanging the stereochemistry of the two

(24) Ashby, M. T.; Alguindigue, S. S.; Khan, M. A. *Inorg. Chim. Acta* **1998**, *270*, 227.
(25) Johnson, C. E.; Bovey, F. A. *J. Chem. Phys.* **1958**, *29*, 1021.

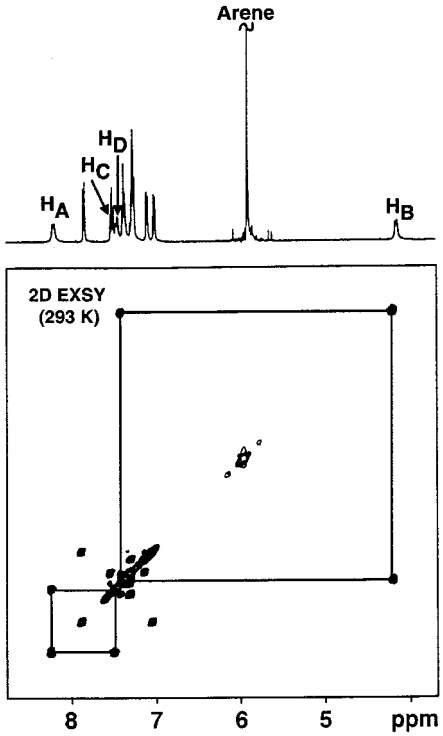

Figure 3. 2D-EXSY spectrum of **1**(M=Ru) at 293 K and 500 MHz that illustrates $H_A \leftrightarrow H_C$ and $H_B \leftrightarrow H_D$ chemical exchange.

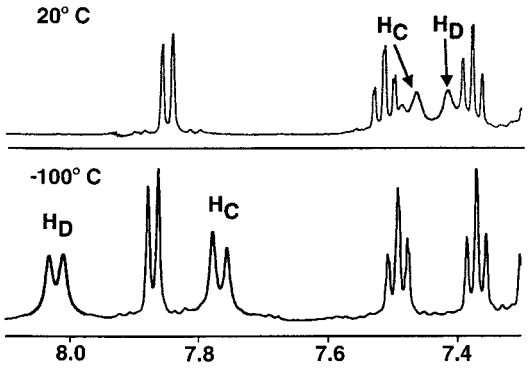

Figure 4. ^{1}H NMR spectra of **1**(M=Ru) at 500 MHz illustrating the temperature dependence of the N−H chemical shifts. Note the relative position of H_C and H_D change in raising the temperature from −100 °C (the temperature at which the 2D-COSY and 2D-NOESY spectra were collected) and 20 °C (the temperature at which the 2D-EXSY spectrum was collected).

"unidentate" ligands (the arene and the chloride). In addition to irregular mechanisms that involve ligand dissociation, such an exchange could be achieved by an intramolecular turnstile-type rearrangement involving a "square planar" transition state.[26] Alternatively, the ligand might undergo atropisomerization[27] either via a *syn* or *anti* transition state (vide infra) (Scheme 2). Finally, it is conceivable that the stereochemistry of the metal and the ligand might invert simultaneously (Scheme 3). Such a mechanism might couple some of the features of the aforementioned mechanisms, perhaps as a result of meshing of the ligands during

(26) Wilkins, R. G. *Kinetics and Mechanism of Reactions of Transition Metal Complexes*; VCH: Weinheim, Germany, 1991; p 355.

(27) March, J. *Advanced Organic Chemistry*, 2nd ed.; McGraw-Hill: New York, 1977; pp 92−93.

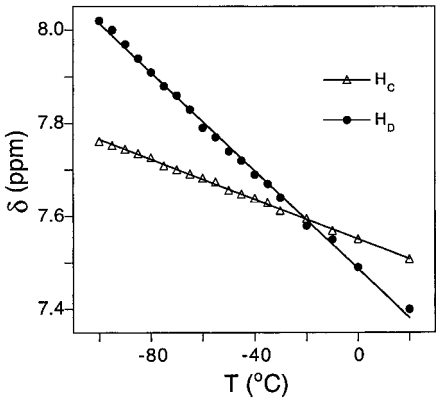

Figure 5. Linear dependence on temperature observed for the NH chemical shifts for **1**(M=Ru) that allow their unambiguous assignment at 20 °C.

Scheme 1

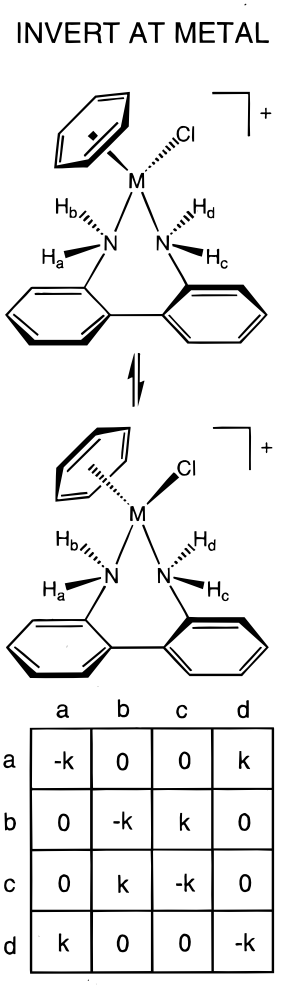

atropisomerization.[28] Having made an assignment of the ^{1}H NMR spectrum, we may distinguish between the three mechanisms of Schemes 1−3.

We conclude from the 2D EXSY NMR spectra of **1**(M=Ru) (Figure 3) that the pairwise exchanges of the N−H resonances on the spin-relaxation time scale are the result of atropisomerization of the dabp ligand. This mechanism is further evidenced by the fact that a single crystal of **1**(M=Ru), which happens to crystallize in a chiral space group ($P2_12_12_1$), fails to exhibit a circular

(28) Iwamura, H.; Mislow, K. *Acc. Chem. Res.* **1988**, *21*, 175.

Scheme 2

INVERT AT LIGAND

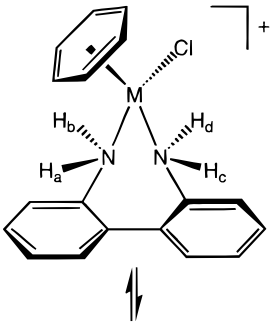

	a	b	c	d
a	-k	0	k	0
b	0	-k	0	k
c	k	0	-k	0
d	0	k	0	-k

Scheme 3

INVERT AT METAL AND LIGAND

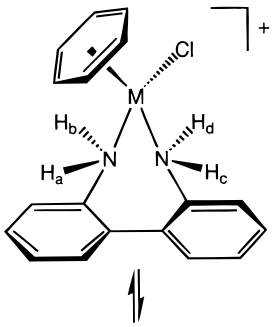

	a	b	c	d
a	-k	k	0	0
b	k	-k	0	0
c	0	0	-k	k
d	0	0	k	-k

dichroism spectrum when dissolved in acetone. Also, an analogous complex of (*S*)-1,1′-binaphthyl-2,2′-diamine (a ligand that is not likely to undergo atropisomerization) fails to reveal a similar pairwise exchange of its N−H resonances.

Discussion

Molecular Structure of 1(M=Ru)**.** The molecular structure of **1**(M=Ru) is largely unremarkable (Table 1). The important stereochemical features have already been pointed out. The observed Ru−N interatomic distances of 2.17 Å for **1**(M=Ru) are comparable to those that have been reported previously for related compounds such as $[(\eta^6\text{-}C_6Me_6)Ru(PMe_3)(H)(NH_2{}^iPr)]^+$ (2.16 Å)[29] and $[(\eta^6\text{-}p\text{-cymene})Ru(H)(H_2N\text{-chelate-}C{=}S)(Cl)]^+$ (2.14 Å).[30] It is noteworthy that the crystal structure of dabp itself has been determined.[31] Intramolecular hydrogen bonding in the free ligand enforces a conformation in its solid-state structure that is quite comparable to the conformation that is observed when dabp is coordinated (e.g., C2−C1−C1′−C2′ = 60.4(11)° in **1**(M=Ru) and the corresponding torsional angle in the free ligand is 59.79(8)°). Together, these metric data suggest the seven-membered chelate ring that is formed when the dabp ligand is coordinated is not highly strained and the Ru−N bonds are quite normal.

Table 1. Selected Interatomic Distances (Å), Angles (deg), and Torsion Angle (deg) for 1(M=Ru)

Ru(1)−N	2.172(6)	H(A)···H(3)	2.34(1)
Ru(1)−N′	2.172(6)	H(B)···H(3)	3.39(1)
Ru(1)−Cl(1)	2.413(2)	H(C)···H(3′)	3.32(1)
Ru(1)−Bz_{cent}[a]	1.662(8)	H(D)···H(3′)	2.27(1)
N−Ru(1)−N′	84.1(2)	Bz_{cent}−Ru(1)−Cl(1)	128.6(3)
N−Ru(1)−Cl(1)	86.2(2)	Bz_{cent}−Ru(1)−N	129.7(4)
N′−Ru(1)−Cl(1)	84.5(2)	Bz_{cent}−Ru(1)−N′	128.0(4)
C(2)−C(1)−C(1′)−C(2′)		60(1)	

[a] Bz_{cent} is the centroid of the arene ligand.

Mechanism of Isomerization. Surprisingly few examples of metal complexes of dabp have been reported,[7−18] although it remains a popular component of chiral Schiff base ligands.[32−36] Despite a report to the

(29) Werner, H.; Kletzin, K.; Zolk, R.; Otto, H. *J. Organomet. Chem.* **1986**, *310*, C11.
(30) Garcia, G.; Solano, I.; Sanchez, G.; Santana, M. D.; Lopez, G.; Casabo, J.; Molins, E.; Miravitlles, C. *J. Organomet. Chem.* **1994**, *467*, 119.
(31) Ottersen, T. *Acta Chem. Scand.* **1977**, *A 31*, 480.
(32) Ligtenbarg, A. G. J.; vandenBeuken, E. K.; Meetsma, A.; Veldman, N.; Smeets, W. J. J.; Spek, A. L.; Feringa, B. L. *J. Chem. Soc., Dalton Trans.* **1998**, 263.
(33) Flanagan, S.; Dong, J.; Haller, K.; Wang, S.; Scheidt, W. R.; Scott, R. A.; Webb, T. R.; Stanbury, D. M.; Wilson, L. J. *J. Am. Chem. Soc.* **1997**, *119*, 8857.
(34) Long, R. C.; Hendrickson, D. N. *J. Am. Chem. Soc.* **1983**, *105*, 1513.
(35) Frydendahl, H.; Toftlund, H.; Becher, J.; Dutton, J. C.; Murray, K. S.; Taylor, L. F.; Anderson, O. P.; Tiekink, E. R. T. *Inorg. Chem.* **1995**, *34*, 4467.
(36) Pignolet, L. H.; Taylor, R. P.; Horrocks, W. D. *J. Am. Chem. Soc.* **1969**, *91*, 5457.

contrary,[8] it is significant that in every case where diastereomers may have been expected upon complexation of dabp, only single isomers were observed.[7,13,14] We have recently synthesized $[Ru(bipy)_2(dabp)]^{2+}$ and found only one diastereomer.[37] It is remarkable that a square-planar Pt(II) complex of dabp has been resolved wherein the dabp ligand appears to be the only source of optical activity and that activity is not lost in solution over a period of hours.[9] With the exception of this latter Pt system, these observations are consistent with the result of the present study that clearly illustrates that atropisomerization of the coordinated dabp ligand is facile for **1**. The observation of one diastereomer could be interpreted as reaction stereospecificity,[7,18] but an alternative explanation is that atropisomerization simply permits equilibration to give the thermodynamic diastereomer. It is noteworthy that the atropisomers of the 6,6′-dimethyl derivative of dabp (dmdabp = 6,6′-dimethyl-2,2′-diamino-1,1′-biphenyl) can be resolved.[38] Metal complexes of dmdabp apparently do not undergo atropisomerization.[14,21]

While the results of this study clearly point to a mechanism for isomerization of **1** that involves atropisomerization of the dabp ligand, the exchange matrix offers no insight into the nature of the transition state. Atropisomerization of the dabp ligand could take place via a mechanism that involves conservation of the M−N bonds and a *syn* transition state:

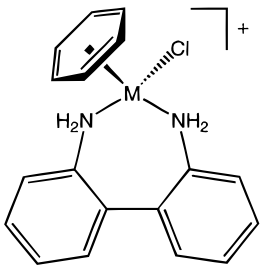

syn

The seven-membered chelate ring and the unfavorable transannular contact of the $-NH_2$ substituents in the 2,2′-positions of the biphenyl group would offer resistance to such an isomerization. Alternatively, one of the M−N bonds might break, which would allow a more comfortable *anti* transition state, albeit with the price of the M−N bond dissociation energy:

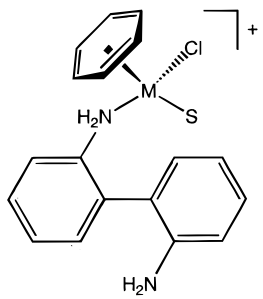

anti

Given the fact the metric data for **1**(M=Ru) point to an entirely normal M−N bond (vide supra), it seems highly likely that the mechanism is one that does not involve the breaking of a M−N bond. Furthermore, such a bond cleavage would give rise to a free aromatic amine group. Such moieties have low inversion barriers at nitrogen, which would result in chemical exchange of the geminal N−H groups, something that is not observed experimentally. Also, M−N bond cleavage would produce a coordinatively unsaturated (16-electron) transient that would likely scramble its stereochemistry at the metal center. Again, this is not indicated. The mechanism of stereoisomerization of **1** therefore appears to be atropisomerization of the dabp ligand via a *syn* transition state. We have previously demonstrated that metals are capable of lowering the barriers of atropisomeric reactions,[22,23] but that does not appear to be the case for dabp (vide infra).

Finally, it is appropriate to compare the barrier for atropiomerization of **1** with barriers that have been previously measured for analogous organic biphenyl systems. For example, the difference in the barrier for atropisomerization[39] of thiepin **3b** (71 kJ mol^{-1}) versus the oxepin **3a** (38 kJ mol^{-1}) presumably reflects the greater plasticity of the bonds about O versus S.[40,41] Another instructive example is the comparison of the hydrocarbon **3c** (50 kJ mol^{-1})[42] versus its 8,8′-dicarboxyl derivative **3d** (98 kJ mol^{-1}).[43] The latter comparison clearly illustrates the importance of substituents in that efforts to resolve **3c** have failed whereas the half-life of racemization of **3d** is 80 min at 33 °C. These few

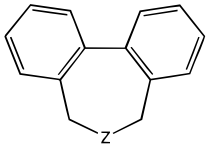

3a: Z = O
3b: Z = S
3c: Z = CH_2
3d: Z = $C(CO_2H)_2$

examples illustrate that the mechanism of isomerization of **1** could not have been predicted a priori since the observed energy barrier is within the ranges expected for the alternative mechanisms that are discussed herein. While the observed energy barriers do not differentiate between inversion at the metal versus inversion at the dabp ligand, the spin tracer experiments (vide supra) clearly demonstrate the mechanism is atropisomerization of the dabp ligand via a *syn* transition state.

Ligand Misdirection. It is also interesting to compare the kinetics of atropisomerization of **1**(M=Ru) with those of **1**(M=Os) (Table 2). We have previously shown that atropisomerization of the 1,1′-biisoquinoline ligand complexes of Ru and Os exhibit an inverse free-energy relationship (Os with its stronger metal−ligand bonds undergoes atropisomerization more readily).[23,44,45] This trend has been attributed to a strengthening of the

(37) Alguindigue, S. S.; Khan, M. H.; Ashby, M. T., unpublished results.
(38) Meisenheimer, J.; Höring, M. *Ber. Dtsch. Chem. Ges.* **1927**, *60*, 1425.
(39) Kurland, R. J.; Rubin, M. B.; Wise, W. B. *J. Chem. Phys.* **1964**, *40*, 2426.
(40) Ashby, M. T.; Sheshtawy, N. A. *Organometallics* **1994**, *13*, 236.
(41) Kutzelnigg, W. *Angew. Chem., Int. Ed. Engl.* **1984**, *23*, 272.
(42) Mullen, K.; Heinz, W.; Klarner, F. G.; Roth, W. R.; Kindermann, I.; Adamczak, O.; Wette, M.; Lex, J. *Chem. Ber.* **1990**, *123*, 2349.
(43) Iffland, D. C.; Siegel, H. *J. Am. Chem. Soc.* **1958**, *80*, 1947.
(44) Ashby, M. T.; Alguindigue, S. S.; Khan, M. A., manuscript in preparation.
(45) Ashby, M. T.; Schwane, J. D.; Daniel, T. A. *Inorg. Chem.*, submitted for publication.

Table 2. Comparison of the Kinetic Data Obtained for the Atropisomerization of the Ru and Os Derivatives of 1[a]

	k_1 (s^{-1})	
temp, °C	M = Ru	M = Os
20	2.71(6)	5.3(6)
25	3.12(7)	
30	3.4(1)	
40	7.2(8)	
50	9.4(9)	

[a] For **1**(M=Ru), $\Delta G_{283\,K}^{\ddagger} = 66.8$ kJ mol^{-1}, and for **1**(M=Os), $\Delta G_{283\,K}^{\ddagger} = 65.3$ kJ mol^{-1}.

metal−biisoquinoline bonds in the *syn* transition state of atropisomerization.[23] In contrast, isomerization reactions that involve a weakening of metal−ligand bonds result in a regular free-energy relationship (Ru faster than Os).[45] We have previously referred to such comparisons between second-row and third-row metal derivative "kinetic element effects".[45] We find for **1** that there is little difference between the rates of atropisomerization of the Ru and Os derivatives. Unfortunately, it was not possible to measure the kinetics of **1**(M=Os) over a range of temperatures, since the rate is too slow below 20 °C and thermal decomposition of **1**(M=Os) was observed above 20 °C. However, assuming the reaction profile of atropisomerization of **1** involves only one stationary state (the transition state), this result suggests the M−N bonds of **1** in the transition state are not significantly perturbed relative to the ground state. This is perhaps not too surprising given the aliphatic nature of the RNH_2 donor of the dabp ligand (in contract to the single-sided nature of the 1,1′-biisoquinoline ligand) and the fact that rehybridization at nitrogen (thereby redirecting the N σ-donor orbital) can compensate for strain placed upon the M−N bond during the atropisomerization process. The similar rates of atropisomerization for **1**(M=Ru) and **1**(M=Os) also lends support to a mechanism that does not involve cleaving one of the M−N (or M−Cl) bonds, but rather a *syn* transition state.

Conclusions

We conclude that the mechanism of isomerization of (η^6-benzene)(δ/λ-1,1′-biphenyl-2,2′-diamine)chlorometal(II) hexafluorophosphate (**1**, metal = ruthenium, osmium) is inversion of stereochemistry at the dabp ligand center via a *syn* transition state. The small "normal" kinetic element effect (KEE = $k_{\text{second row}}/k_{\text{third row}}$) of 0.51 suggests the metal−ligand bond strengths are not perturbed significantly during the stereoisomerization. These results contrast with earlier reports that it is possible to resolve conformational isomers of metal complexes of dabp.[8,9]

Experimental Section

Procurement and Sample Preparation. Acetone-d_6 was dried with molecular sieves and distilled before use. [(η^6-C_6H_6)-$Ru(Cl)_2]_2$,[46] (η^6-C_6H_6)$Os(NCCH_3)(Cl)_2$,[47] and 1,1′-biphenyl-2,2′-diamine (dabp)[48] were synthesized using literature methods. (*S*)-1,1′-Binaphthyl-2,2′-diamine (dabn) was used as received from Aldrich. ^{1}H NMR spectra were recorded on a Varian XL-500 using residual acetone-d_5 (2.04 ppm) as an internal standard. The NMR samples were prepared in tubes that had been glass-blown onto Schlenk adapters. The solutions were freeze−pump−thawed, and the tubes were flame-sealed under vacuum. Combustion analyses were carried out by Midwest Microlab.

Synthesis of [(η^6-C_6H_6)Ru(dabp)(Cl)]PF_6 (1(M=Ru)). [(η^6-C_6H_6)$Ru(Cl)_2]_2$ (144 mg, 0.29 mmol) and dabp (150 mg, 0.82 mmol) were dissolved in MeOH (20 mL). The resulting solution was freeze−pump−thawed and left under vacuum, and the flask was placed in a 70 °C oil bath for 30 min. After the solution was cooled to room temperature, excess NH_4PF_6 was added to precipitate the product. The resulting orange crystals were filtered, washed with MeOH, and dried under vacuum (213 mg, 0.39 mmol, 68%). ^{1}H NMR (acetone-d_6, 500 MHz, 20 °C): δ 8.25 (br s, 1H, H_a), 7.84 (d, 1H, J = 8 Hz, H_3), 7.52 (t, 1H, J = 8 Hz, H_4), 7.47 (br s, 1H, H_c), 7.43 (br s, 1H, H_d), 7.38 (t, 1H, J = 8 Hz, H_5), 7.27 (m, 3H, $H_{4',5',6}$), 7.10 (d, 1H, J = 8, $H_{6'}$), 7.02 (d, 1H, J = 8 Hz, $H_{3'}$), 5.92 (s, 6H, C_6H_6), 4.17 (br s, 1H, H_b). ^{1}H NMR (acetone-d_6, 500 MHz, −88 °C): δ 8.74 (d, 1H, J = 11 Hz, H_a), 7.95 (d, 1H, J = 11 Hz, H_d), 7.87 (d, 1H, J = 8 Hz, H_3), 7.76 (d, 1H, J = 11 Hz, H_c), 7.50 (t, 1H, J = 8 Hz, H_4), 7.37 (t, 1H, J = 8 Hz, H_5), 7.29 (t, 1H, J = 8 Hz, $H_{4'}$), 7.24 (m, 2H, $H_{5',6}$), 7.04 (d, 1H, J = 8 Hz, $H_{6'}$), 6.94 (d, 1H, J = 8 Hz, $H_{3'}$), 5.91 (s, 6H, C_6H_6), 4.60 (d, 1H, J = 11 Hz, H_b). Anal. Calcd for $C_{19}H_{22}ClF_6N_2OPRu$ (**1**(M=Ru)·MeOH): C, 39.61; H, 3.85. Found: C, 38.68; H, 3.90. HRMS (FAB): *m/e* calcd for M^+ ($C_{18}H_{18}ClN_2Ru$), 399.0195; found, 399.0215 ± 0.013. The stoichiometry of methanol in the crystalline product was confirmed by ^{1}H NMR in CD_2Cl_2 and X-ray diffraction.

Synthesis of [(η^6-C_6H_6)Os(dabp)(Cl)]PF_6 (1(M=Os)). (η^6-C_6H_6)$Os(NCCH_3)(Cl)_2$ (75 mg, 0.19 mmol) and dabp (56 mg, 0.30 mmol) were dissolved in MeOH (20 mL). The resulting solution was freeze−pump−thawed and left under vacuum, and the flask was placed in a 70 °C oil bath for 20 h. After the solution was cooled to room temperature, excess NH_4PF_6 was added, the volatiles were removed with a rotary evaporator, and the residue was dissolved in CH_2Cl_2. The resulting solution was filtered, and the volatiles were removed under vacuum to afford **1**(M=Os) as a brown solid (75 mg, 0.12 mmol, 60%). ^{1}H NMR (acetone-d_6, 500 MHz, 20 °C): δ 8.72 (br s, 1H, H_a), 7.92 (br s, 1H, H_c), 7.77 (d, 1H, J = 8 Hz, H_3), 7.76 (br s, 1H, H_d), 7.52 (t, 1H, J = 8 Hz, H_4), 7.36 (m, 3H, $H_{4',5',5}$), 7.30 (d, 1H, J = 8, H_6), 7.20 (d, 1H, J = 8 Hz, $H_{6'}$), 7.15 (d, 1H, J = 8 Hz, $H_{3'}$), 6.21 (s, 1H, C_6H_6), 5.69 (br s, 1H, H_b). ^{1}H NMR (acetone-d_6, 500 MHz, −90 °C): δ 9.23 (br s, 1H, H_a), 8.32 (br s, 1H, H_d), 8.17 (br s, 1H, H_c), 7.78 (d, 1H, J = 8 Hz, H_3), 7.49 (t, 1H, J = 7 Hz, H_4), 7.33 (m, 3H, $H_{4',5',5}$), 7.26 (d, 1H, J = 7 Hz, H_6), 7.12 (d, 1H, J = 7 Hz, $H_{6'}$), 7.05 (d, 1H, J = 7 Hz, $H_{3'}$), 6.17 (s, 1H, C_6H_6), 6.15 (br s, 1H, H_b). The sample that was submitted for combustion analysis was recrystallized from acetone/ether. The stoichiometry of acetone in the crystalline product was confirmed by ^{1}H NMR in CD_2Cl_2. Anal. Calcd for $C_{21}H_{24}ClF_6N_2OPOs$ (**1**(M=Os)·acetone): C, 36.58; H, 3.51. Found: C, 37.30; H, 3.51.

Synthesis of [(δ^6-C_6H_6)Ru(dabn)(Cl)]PF_6 (2). Compound **2** was synthesized using a procedure analogous to the one that was used to synthesize **1**(M=Ru) (121 mg, 0.19 mmol, 65%). ^{1}H NMR (acetone-d_6, 500 MHz, 20 °C): δ 8.44 (d, 1H, J = 9), 8.25 (q, 2H, J = 8), 8.10 (d, 1H, J = 8), 7.94 (m, 2H), 7.62 (d, 1H, J = 10 Hz), 7.54 (t, 1H, J = 8 Hz), 7.47 (m, 2H), 7.35 (m, 2H), 7.24 (t, 1H, J = 8 Hz), 6.98 (d, 1H, J = 8 Hz), 6.90 (d, 1H, J = 8), 5.96 (s, 6H), 4.37 (d, 1H, J = 10 Hz). Anal. Calcd for $C_{26}H_{22}ClF_6N_2PRu$: C, 48.49; H, 3.45. Found: C, 47.66; H, 3.50.

X-ray Diffraction Study of 1(M = Ru). Crystallographic solution and refinement procedures are summarized in Table 3. Diffraction-quality crystals were grown from the reaction mixture. A Siemens P4 four-circle diffractometer was employed to collect a $\theta/2\theta$ data set at 188 K using Mo Kα radiation

(46) Zelonka, R. A.; Baird, M. C. *Can. J. Chem.* **1972**, *50*, 3063.
(47) Freedman, D. A.; Magneson, D. J.; Mann, K. R. *Inorg. Chem.* **1995**, *34*, 2617.
(48) Smith, W. B. *J. Heterocycl. Chem.* **1987**, *24*, 745.

Table 3. Crystal Data for Compound 1(M=Ru)

formula	$C_{19}H_{22}ClF_6N_2OPRu$
fw	575.88
space group	$P2_12_12_1$
cryst syst	orthorhombic
a, Å	9.9001(13)
b, Å	11.099(2)
c, Å	19.462(2)
V, Å^3	2138.6(5)
T, K	188(2)
Z	4
D_{calcd}, g mL^{-1}	1.79
μ, mm^{-1}	1.00
cryst size, mm^3	0.18 × 0.26 × 0.26
no. of indep rflns	2327
θ range (deg)	2.09−25.01
final R indices[a] ($I > 2\sigma(I)$)	
R1	0.0460
wR2	0.1166
R indices (all data used in refinement)	
R1[a]	0.0509
wR2[b]	0.1296
GOF[c]	1.141

[a] $R1 = \sum||F_o| - |F_c||/\sum|F_o|$. [b] $wR2 = [\sum[w(F_o^2 - F_c^2)]/\sum[w(F_o^2)^2]]^{1/2}$; $w = 1/\sum[\sigma^2(F_o)^2 + (aP)^2 + (bP)]$, $P = (F_o)^2[1/3 + [2(F_o)^2/3]]$ for $F_o^2 \geq 0$ (otherwise zero). [c] $GOF = [\sum[w(F_o^2 - F_c^2)/(n - m)]^{1/2}$, where n = no. of reflections observed and m = no. of parameters.

(0.710 73 Å). The data were corrected for Lorentz and polarization effects, and an empirical absorption correction based on ψ-scans was applied. The structure was solved by direct methods using the Siemens SHELXTL system and refined by full-matrix least squares on F^2 using all of the reflections.[49] Atomic coordinates and isotropic vibrational parameters for **1**(M=Ru) are given in the Supporting Information. Selected interatomic distances, angles, torsion angles, and other metric parameters are given in Table 1. A diagram showing the thermal ellipsoids (at the 50% level) of the molecule and labeling scheme is given in Figure 1. The dashed lines indicate close hydrogen atom contacts that are relevant to the NMR experiments (vide supra). Other data are available as Supporting Information. The structure of **1**(M=Ru) was successfully solved and refined in the chiral space group $P2_12_12_1$. Statistical tests carried out after structure refinement indicate the structure presented herein is the correct enantiomorph of the particular crystal that was selected for data collection from the presumably racemic mixture. The asymmetric unit contains one $[(\eta^6\text{-}C_6H_6)Ru(dabp)Cl]^+$ cation, one PF_6^- anion, and a methanol solvent molecule. One of the fluorine atoms (F_3) of the PF_6^- anion and the oxygen atom of the methanol solvent molecule may exhibit weak H-bond contact with one of the nitrogen atoms (N) of the cation. This contact is illustrated in a unit cell diagram that is available in the Supporting Information.

Temperature Dependence and Assignment of ^{1}H NMR Spectrum of 1. Scalar coupling relationships between the protons were obtained using ^{1}H−^{1}H double-quantum-filtered homonuclear correlation spectroscopy (dqf-COSY)[50] at −88 °C for **1**(M=Ru) and at −90 °C for **1**(M=Os), conditions under which chemical exchange is slow (e.g., Figure 2, top). The stereochemical relationship between the hydrogen atoms bound to the two nitrogen atoms was established by phase-sensitive nuclear Overhauser spectroscopy (NOESY) at −88 °C (M = Ru) and at −90 °C (M = Os), (e.g. Figure 2, bottom). As is explained in the Results, the 2D COSY, NOESY, and EXSY spectra are completely consistent with this assignment. It is important to note, however, that the N−H protons of **1**(M=Ru,Os) exhibit temperature-dependent chemical shifts (Figures 4 and 5). Thus, the relative chemical shifts of the N−H protons change from the temperature at which their assignments were made (−88 °C for **1**(M=Ru) and −90 °C for **1**(M=Os)), to the temperature at which the rates of atropisomerization were measured (20 °C for **1**(M=Ru,Os)).

Symmetry of Magnetic Exchange by 2D EXSY. The two-dimensional exchange spectroscopy (2D EXSY) pulse sequence is essentially the same as that used for phase-sensitive nuclear Overhauser effect spectroscopy (NOESY): d_1, $\pi/2$, d_2, $\pi/2$, τ_m, $\pi/2$, aq.[51] However, whereas the aforementioned NOESY spectrum was collected at −88 °C (M = Ru) and at −90 °C (M = Os), temperatures at which chemical exchange is slow on the spin-relaxation time scale, the 2D EXSY was collected at 20 °C (M = Ru, Os), a temperature at which chemical exchange is slow on the NMR time scale (i.e., apparently static spectra are obtained) but fast on the spin-relaxation time scale. The relaxation delay d_1 was set equal to 5 times the longest T_1 to allow complete longitudinal relaxation between pulses. Because of the long d_1 delay time, a homospoil−$\pi/2$−homospoil presequence was unnecessary. A mixing time of $\tau_m = 0.5$ s was used to obtain the spectrum of Figure 3; however, varying the τ_m value had little effect on the qualitative features of the spectrum. The spectrum of Figure 3 only illustrates the positive peaks; therefore, the cross-peaks corresponding to chemical exchange are observed. Weak negative cross-peaks that correspond to NOE coupling were also observed. Increasing the threshold of the spectrum of Figure 3 reveals positive cross-peaks that result from zero-quantum coherence (zero-quantum-filtered COSY), but the latter peaks are substantially weaker than the cross-peaks that are attributed to chemical exchange. Quantitative rate information can be obtained from 2D EXSY spectroscopy. One disadvantage to this method is that the cross-peak and diagonal peak intensities need to be measurable. Errors in these measurements are propagated into the rate calculations.[52] Another disadvantage is that several mixing times must be used, leading to the need for large amounts of instrument time.[53] The advantage to this method is in calculating rate constants in multisite systems. For a two-site system such as this one, there is no advantage in using 2D EXSY to determine rate constants. For such systems, line-shape analysis and magnetization-transfer experiments are preferable.[54]

Rates of Atropisomerization by Spin Inversion Transfer (SIT) NMR. SIT rate data were obtained using the standard pulse sequence: d_1, $\pi/2$, d_2, $\tau/2$, τ_m, $\pi/2$, aq.[55−58] The transmitter offset frequency was set equal to ν_A, the frequency of the nucleus to be inverted. The relaxation delay d_1 was set equal to 5 times the longest T_1 to allow complete longitudinal relaxation between pulses. The second delay was set equal to $1/(2|\nu_A - \nu_B|)$, where $|\nu_A - \nu_B|$ is the frequency difference between the nucleus to be inverted and the exchanging nucleus. The mixing time τ_m was typically varied from 0.001 s to about $5T_1$. The 90° pulse width was determined experimentally prior to each kinetics run. The rate constants and T_1 relaxation times were obtained by nonlinear least-squares fit of the equations that describe the recovery of the inverted

(49) SHELXTL Software Package for the Determination of Crystal Structures; Siemens Analytical X-ray Instruments, Inc., Madison, WI, 1995.
(50) Rance, M.; Sorensen, O. W.; Bodenhausen, G.; Wagner, G.; Ernst, R. R.; Wüthrich, K. *Biochem. Biophys. Res. Commun.* **1983**, *117*, 479.
(51) Abel, E. W.; Coston, T. P. J.; Orrell, K. G.; Sik, V.; Stephenson, D. *J. Magn. Reson.* **1986**, *70*, 34.
(52) Macura, S.; Farmer, B. T.; Brown, L. R. *J. Magn. Res.* **1986**, *70*, 493.
(53) Heise, J. D.; Raftery, D.; Breedlove, B. K.; Washington, J.; Kubiak, C. P. *Organometallics* **1998**, *17*, 4461.
(54) Perrin, C. L.; Dwyer, T. J. *Chem. Rev.* **1990**, *90*, 935.
(55) Alger, J. R.; Prestegard, J. H. *J. Magn. Reson.* **1977**, *27*, 137.
(56) Kuchel, P. W.; Chapman, B. E. *J. Theor. Biol.* **1983**, *105*, 569.
(57) Robinson, G.; Kuchel, P. W.; Chapman, B. E. *J. Magn. Reson.* **1985**, *63*, 314.
(58) Bellon, S. F.; Chen, D.; Johnston, E. R. *J. Magn. Reson.* **1987**, *73*, 168.

resonance (A) and the effect on the resonance that corresponds to the hydrogen atom(s) that are undergoing chemical exchange (B):

$$A \underset{k_b}{\overset{k_a}{\rightleftharpoons}} B$$

The effective first-order rate constants are represented as the sum of the two first-order rate constants for the pathways that lead to a loss of magnetization, chemical exchange and spin−lattice relaxation:

$$k_a^{eff} = k_a + 1/T_{1a} \quad (1)$$

The present case is a special one for which $K = 1$, $k_a = k_b$, and $T_{1a} \approx T_{1b}$. Therefore, the usual Block equations for SIT may be simplified as

$$M_z^A(t) = c_1 \exp(-t/T_1) + c_2 \exp(-t(2k + 1/T_1)) + M_\infty^A \quad (2)$$

$$M_z^B(t) = c_1 \exp(-t/T_1) - c_2 \exp(-t(2k + 1/T_1)) + M_\infty^B \quad (3)$$

where c_1 and c_2 are defined by

$$c_1 = (M_0^A - M_\infty^A + M_0^B - M_\infty^B)/2 \quad (4)$$

$$c_2 = (M_0^A - M_\infty^A + M_0^B - M_\infty^B)/2 \quad (5)$$

The data consisting of peak amplitude versus delay time τ_m were analyzed by fitting eqs 2 and 3 to the experimental data. The numerical analysis was performed with the nonlinear least-squares regression program SPIRAL.[59] Using the known values of M_∞^A and M_∞^B, the nonlinear regression yielded values and estimated errors for k_{obs}, M_0^A, M_0^B, and T_1. Typical fits for spin transfer and inversion recovery are illustrated in the Supporting Information. The kinetic data (k_{obs}'s) that were obtained from the SIT experiments and the conditions that were employed for each experiment are summarized in Table 2.[60]

Acknowledgment. The financial support of the National Science Foundation (Grant No. CHE-9612869) and the donors of the Petroleum Research Fund, administered by the American Society, is gratefully acknowledged. S.S.A. is a Department of Education GAAN Fellow.

Supporting Information Available: Cell packing diagram of **1**(M=Ru) illustrating intermolecular hydrogen bonding, tables of fractional coordinates of the non-hydrogen atoms, anisiotropic thermal parameters, hydrogen atom parameters, and complete distances and angles for **1**(M=Ru), a fit of sample SIT data for **1**(M=Ru), and a figure similar to Figure 5 for **1**(M=Os). This material is available free of charge via the Internet at http://pubs.acs.org.

OM990332G

(59) Jones, A. *Comput. J.* **1970**, *13*, 301.
(60) Green, M. L. H.; Wong, L.-L.; Sella, A. *Organometallics* **1992**, *11*, 2660.